ResearchGate

See discussions, stats, and author profiles for this publication at: https://www.researchgate.net/publication/223968433

Porous Doped Silicon Nanowires for Lithium Ion Battery Anode with Long Cycle Life

ARTICLE *in* NANO LETTERS · APRIL 2012

Impact Factor: 13.59 · DOI: 10.1021/nl300206e · Source: PubMed

CITATIONS
233

READS
125

4 AUTHORS, INCLUDING:

Mingyuan Ge
University of Southern California
43 PUBLICATIONS **1,516** CITATIONS
SEE PROFILE

Jiepeng Rong
University of Southern California
21 PUBLICATIONS **960** CITATIONS
SEE PROFILE

Xin Fang
University of Southern California
31 PUBLICATIONS **806** CITATIONS
SEE PROFILE

Available from: Mingyuan Ge
Retrieved on: 29 January 2016

NANO LETTERS

Letter

pubs.acs.org/NanoLett

Porous Doped Silicon Nanowires for Lithium Ion Battery Anode with Long Cycle Life

Mingyuan Ge,[†,§] Jiepeng Rong,[†,§] Xin Fang,[†] and Chongwu Zhou*[,‡]

[†]Department of Electrical Engineering and [‡]Department of Chemical Engineering and Materials Science, University of Southern California, Los Angeles, California 90089, United States

Supporting Information

ABSTRACT: Porous silicon nanowires have been well studied for various applications; however, there are only very limited reports on porous silicon nanowires used for energy storage. Here, we report both experimental and theoretical studies of porous doped silicon nanowires synthesized by direct etching of boron-doped silicon wafers. When using alginate as a binder, porous silicon nanowires exhibited superior electrochemical performance and long cycle life as anode material in a lithium ion battery. Even after 250 cycles, the capacity remains stable above 2000, 1600, and 1100 mAh/g at current rates of 2, 4, and 18 A/g, respectively, demonstrating high structure stability due to the high porosity and electron conductivity of the porous silicon nanowires. A mathematic model coupling the lithium ion diffusion and the strain induced by lithium intercalation was employed to study the effect of porosity and pore size on the structure stability. Simulation shows silicon with high porosity and large pore size help to stabilize the structure during charge/discharge cycles.

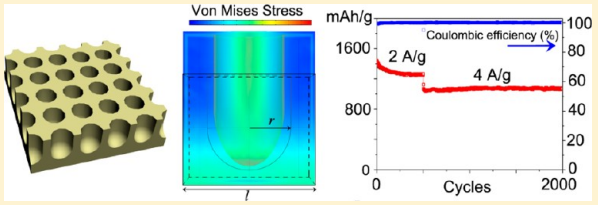

KEYWORDS: *Porous silicon nanowire anode, structure stability, alginate binder, high current rate*

The ever increasing demand in energy storage has stimulated significant interest in lithium ion battery research. The lithium ion battery is one of the most promising systems which is efficient in delivering energy, light in weight, and environmentally benign.[1−5] Existing lithium ion batteries using graphite as the anode have already been widely used in mobile applications; however, it is still urgent and important to develop new battery systems with larger specific capacity and higher power density for applications in mobile devices, hybrid electric vehicles (HEVs), and plug-in hybrid electric vehicles (PHEVs).[6] For anode materials, silicon is known to have the highest theoretical specific capacity (4200 mAh/g).[7] Comparing with graphite (372 mAh/g), which is currently used, silicon is considered to be the anode material for the next generation lithium ion batteries. However, silicon is easy to pulverize and loses its capacity due to large volume change (around 300%) during repeated insertion and extraction of lithium ions.[8] In addition, silicon has low electron conductivity (when undoped) and low diffusivity for lithium ions. The above-mentioned drawbacks set hindrances for silicon to be used in high power density batteries. Decreasing the silicon dimensions to submicrometers or nanometers, to a large extent, solves the problems mentioned above. Extensive studies on silicon thin films,[9,10] silicon nanowires,[11−14] nanoparticles,[15,16] nanotubes,[17−19] and porous structures[20−23] have shown very encouraging results when used as anode materials in lithium ion batteries.

For half cells, which use silicon as the working electrode and lithium metal as the counter electrode, the battery voltage is determined by the chemical potential difference of lithium ions at the interface between electrolyte and silicon. The charge process finishes when the lithium-rich phase ($Li_{22}Si_5$ at high temperature and $Li_{15}Si_4$ at room temperature)[24] is formed at the silicon surface, and the discharge process ends when all the lithium ions are extracted from the very outer surface of silicon, regardless of whether the inner part of silicon has fully participated in the lithiation/delithiation process or not. The charge/discharge capacities are related to both the transfer of lithium ions between the electrolyte and silicon interface and the diffusion of lithium ions inside silicon. This explains why usually only a portion of the theoretical capacity can be reached, and the problem of reduced capacity gets exacerbated when the battery runs at a higher charge/discharge rate. Therefore, obtaining uniform lithium ion concentration in silicon at a fast charge/discharge rate remains a challenge to be addressed. In addition, at very high charge/discharge rates, low electron conductivity of intrinsic silicon would also compromise battery performance and result in reduced capacity. To enable silicon to work at high charge/discharge rates, it is therefore very important to have the following properties: a large surface area accessible to the electrolyte, a short diffusion length for lithium ions, a large space available to accommodate volume change, and a high electron conductivity.

Here we report both the experimental and the theoretical study of porous doped silicon nanowires synthesized by direct etching of boron-doped silicon wafers. The obtained porous

Received: January 17, 2012
Revised: April 2, 2012
Published: April 9, 2012

ACS Publications © 2012 American Chemical Society

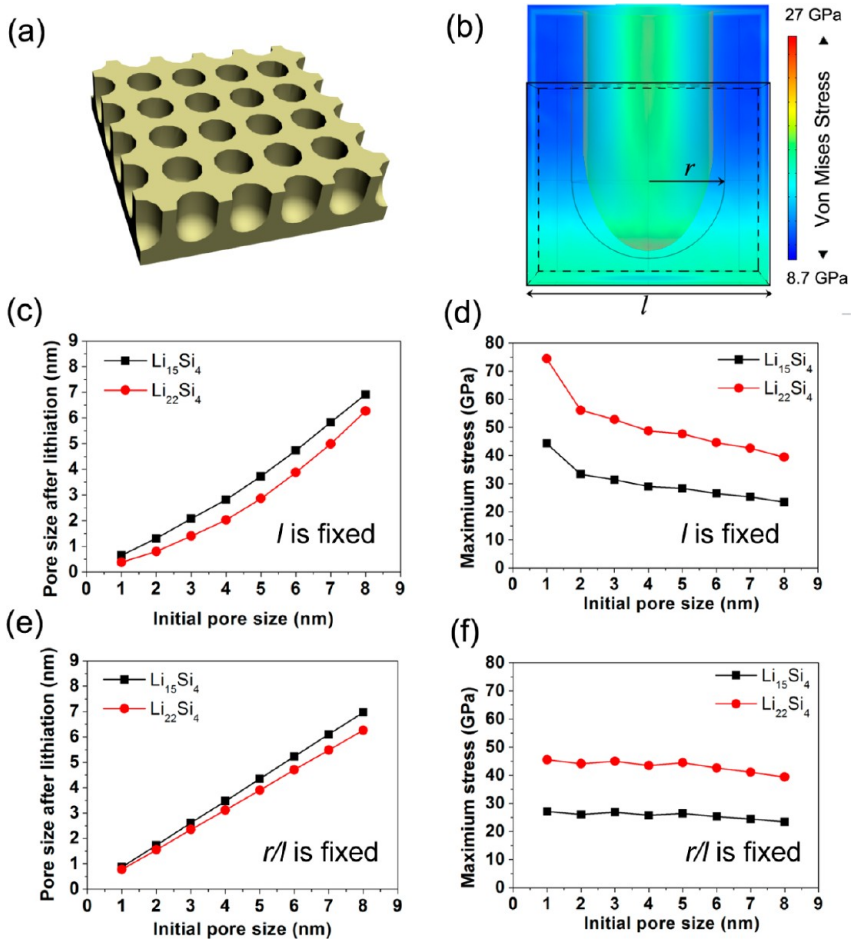

Figure 1. (a) Schematic diagram of a porous silicon structure. (b) One unit of the porous structure used for theoretical simulation and analysis. (c) Pore size before and after lithiation and (d) corresponding maximum stress at fixed pore-to-pore distance (l = 12 nm). (e) Pore size before and after lithiation and (f) corresponding maximum stress vs initial pore size at fixed pore/edge ratio (r/l = 1/3).

silicon nanowires have all of the above properties. In addition, we used a commercially available alginic acid sodium salt as the binder (denoted alginate binder), which has a viscosity of 2000 cP at 2 wt % but so far has not been fully explored for battery study. The porous silicon nanowires exhibit superior electrochemical performance and long cycle life as an anode material in lithium ion batteries when combined with the alginate binder. Even after 250 cycles, the capacity remains stable above 2000, 1600, and 1100 mAh/g at current rates of 2, 4, and 18 A/g, respectively. Our best battery has recorded 2000 cycles with a capacity remaining above 1000 mAh/g. Simulation has been carried out to illustrate strain induced by lithium ion diffusion, as stated below.

A mathematic model[25,26] coupling the lithium ion diffusion and the strain induced by lithium intercalation was employed to study the effects of porosity and pore size on the structure stability. Figure 1a schematically shows the porous structure, and calculation and analysis were carried out on one unit (Figure 1b) of the structure in Figure 1a. Insertion of lithium would generate stress in the silicon matrix, and the strain induced by stress not only deforms the structure (expansion) but also compromises the lithium diffusion. The pore size evolution after lithium ion intercalation to $Li_{22}Si_5$ and $Li_{15}Si_4$ at fixed pore-to-pore distance (l = 12 nm) was presented in Figure 1c. It shows that the pore diameter after lithium intercalation decreases with decreasing initial pore size. The maximum stress around the pore increases as we decrease the initial pore size (Figure 1d), which would act as a source of fracture. In another case, we fix the porosity by means of fixing the ratio of initial pore radius (r) and the pore-to-pore distance (l). Figure 1e shows the correlation of pore sizes before and after lithiation, and there is almost no change in the maximum stress at different pore sizes (Figure 1f). Generally speaking, decreasing r/l ratio to a lower value (low porosity) would increase maximum stress, and a smaller initial pore results in higher maximum stress around the pore. Therefore, obtaining silicon with high porosity and large pore size would help to stabilize the structure during the charge/discharge process. In order to verify the assumption, we synthesized porous silicon nanowires with large pores to check their electrochemical performance.

Porous Si nanowires were prepared according to previous reports.[27,28] Briefly, boron-doped Si wafers (resistivity <5 mΩ·cm) were immersed in an etchant solution containing 5 M hydrofluoric acid (HF) and 0.02 M silver nitrite ($AgNO_3$) for 3 h. Porous nanowires were washed by deionized water (DI-H_2O), concentrated nitric acid (HNO_3), and DI-H_2O again, sequentially, and then collected by scratching the wafers using a blade. We note that doping is necessary for getting a porous structure, and without doping, we can only get solid silicon nanowire. Figure 2 shows scanning electron microscopy (SEM) (Figure 2a) and transmission electron microscopy (TEM) (Figure 2b–d) images of porous Si nanowires. The nanowires

dx.doi.org/10.1021/nl300206e | Nano Lett. 2012, 12, 2318–2323

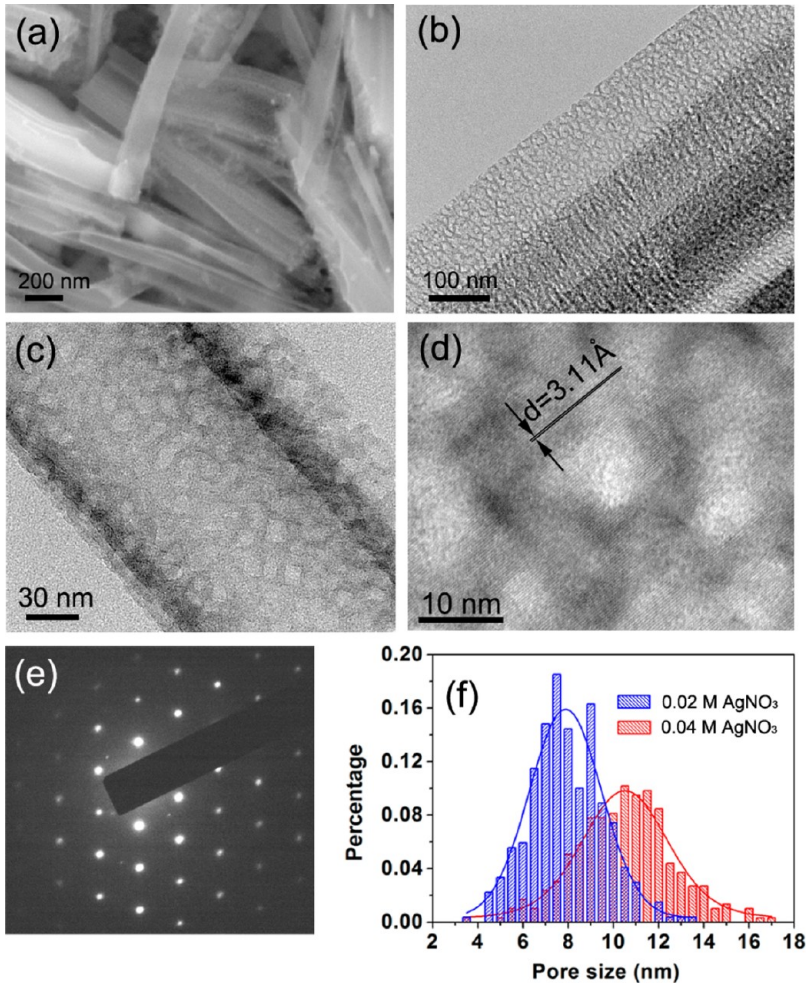

Figure 2. (a) SEM and (b) TEM images of porous Si nanowires etched with 0.02 M $AgNO_3$. (c,d) HRTEM image of a nanowire in (b). (e) SAED pattern of a single porous silicon nanowire. (f) Pore size distribution of porous Si nanowires etched with 0.02 and 0.04 M $AgNO_3$, respectively.

are highly porous at the surface, with pore diameter and wall thickness both around 8 nm (Figure 2b,c). The high-resolution TEM (HRTEM) image in Figure 2d shows the nanowires are crystalline with clear lattice fringes corresponding to a Si (111) lattice. The crystalline structure was also confirmed by the spot pattern in selected area electron diffraction (SAED) taken on a single porous nanowire, as shown in Figure 2e. The pore size could be tailored by reacting with $AgNO_3$ at different concentrations. Etchants containing 0.02 and 0.04 M $AgNO_3$ gave pores with mean diameters of 7.8 ± 0.1 and 10.5 ± 0.1 nm (Figure 2f), respectively, based on statistical analysis of the TEM images. The boron dopants provide defective sites facilitating the etching process which leaves holes on the silicon nanowire surface. The etching process was described as two simultaneous electrochemical reactions:[28]

$$4Ag^+ + 4e^- \rightarrow 4Ag$$

$$Si + 6F^- \rightarrow [SiF_6]^{2-} + 4e^-$$

To test the electrochemical performance of porous silicon nanowires, two-electrode coin cells using porous silicon nanowires as the anode and lithium metal as the counter electrode were fabricated. The Si mass loading is around 0.3 mg/cm^2, which is comparable to the amount previously reported for silicon nanowires.[11] Figure 3a shows the voltage profile in the charge (lithiation) and discharge (delithiation) process in the potential window of 0.01−2.0 V vs Li^+/Li. The first cycle at a current rate of 0.4 A/g shows charge and discharge capacities of 3354 and 3038 mAh/g, respectively. Cycles from the 20th and thereafter run at a current density of 2 A/g show capacity degradation of only about 9% per 100 cycles. After 200 cycles, the capacity is still above 1960 mAh/g, indicating good structure stability of porous Si nanowires. Transition from crystalline Si to an amorphous structure during cycling was confirmed by cyclic voltammetry ($C-V$) curves at the first and second charge/discharge cycles (Figure 3b). During the second cycle, the peak at 0.15 V, which is absent at the first cycle at cathodic branch (lithiation), indicates the crystal-to-amorphous transition.[29]

Figure 3c shows the charge/discharge capacity and the Coulombic efficiency at different current rates. The capacity maintains above 3400, 2600, 2000, 1900, 1700, and 1300 mAh/g at current densities of 0.6, 1.2, 2.4, 3.6, 4.8, and 9.6 A/g. The Coulombic efficiency is around 90% during the first several cycles which may be very well due to the large surface area of porous Si that needs a longer time to form a stable solid electrolyte interface (SEI) layer. After 20 cycles, the Coulombic efficiency reaches above 99.5% at each different current rate cycling step. The current rate, charging/discharging time, and average specific capacity at different current rates are summarized in Table 1. It indicates that even at high current rates (2.4 C = 9.6 A/g at step 6), charging/discharging finished

dx.doi.org/10.1021/nl300206e | Nano Lett. 2012, 12, 2318−2323

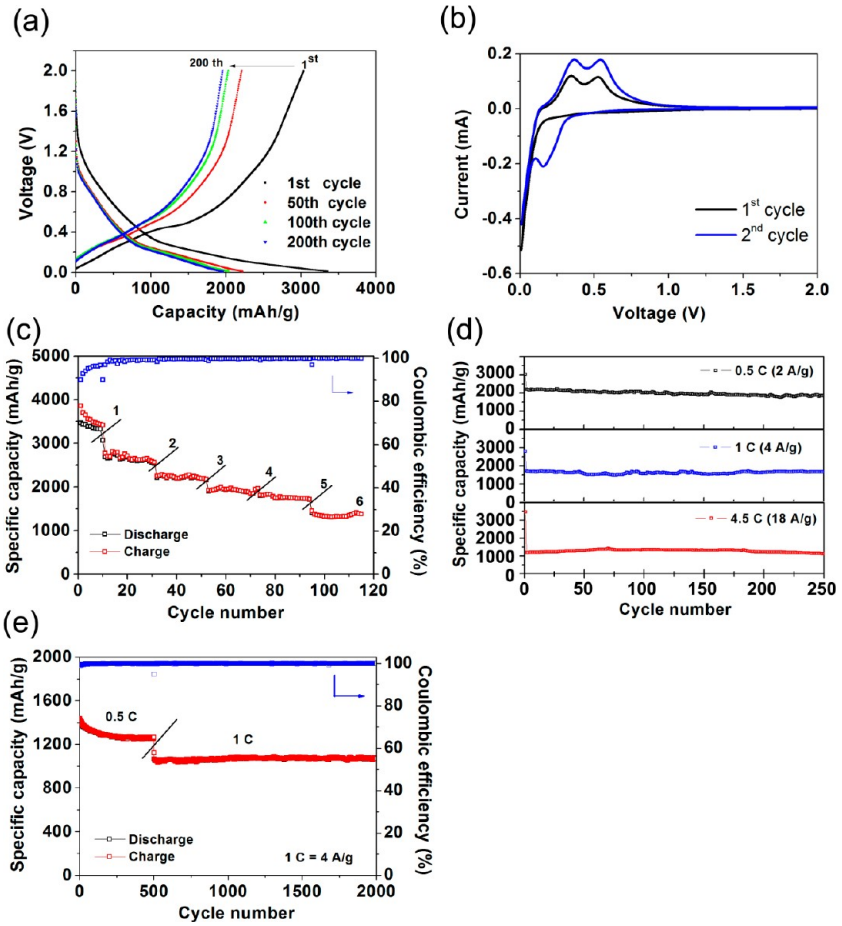

Figure 3. Electrochemical performance of a battery using porous silicon nanowires as the anode and lithium metal as the current collector. (a) Charge/discharge profile within a voltage window of 0.01−2 V vs Li^+/Li for the first cycle at a current rate of 0.4 A/g and the 50th, 100th, and 200th cycles at 2 A/g. (b) Cyclic voltammetry curves of porous silicon nanowire electrode for the first and second cycles using a voltage window 0.01−2 V at rate of 0.1 mV/s. (c) Charge/discharge capacity and Coulombic efficiency of porous silicon nanowire electrode at current rates of 0.6, 1.2, 2.4, 3.6, 4.8, and 9.6 A/g. (d) Charge/discharge capacity of a porous silicon nanowire electrode at current rates of 2, 4, and 18 A/g for 250 cycles. (e) Charge/discharge capacity of a porous silicon nanowire electrode at current rates of 2 A/g (0.5 C) and 4 A/g (1 C) with an additional 2000 cycles.

Table 1. Detailed Information of Battery Performance Corresponding to Figure 3c

step number	number of cycle	charging time	charging rate (1 C = 4 A/g)	average specific capacity (mA h/g)
1	10	6 h	0.15 C	>3400
2	20	2 h	0.30 C	>2600
3	20	1 h	0.60 C	>2000
4	20	40 min	0.90 C	>1900
5	20	30 min	1.20 C	>1700
6	20	10 min	2.40 C	>1300

within 10 min still gave capacity above 1300 mAh/g, equivalent to 38% of capacity using 0.15 C (step 1). Figure 3d shows a long cycle performance at charging/discharging rate of 0.1 C for the first cycle and 0.5 C, 1 C, and 4.5 C for an additional 250 cycles, which shows stable capacities around 2000, 1600, and 1100 mAh/g, respectively. Capacity degradation is almost negligible in each case, demonstrating good stability of the porous silicon structure. The battery shown in the top panel of Figure 3d has been retested with 0.5 C and then 1 C current rate after one month. It shows that the capacity remains above 1000 mAh/g after additional 2000 cycles (Figure 3e). Our result compares well with previously reported porous silicon structures.[20,21] As reported before, three-dimensional porous silicon particles[20] showed a capacity around 2500 mAh/g at a current rate of 0.5 C for 100 cycles, with Coulombic efficiency >98% at 0.5 C, while interconnected silicon hollow nanospheres[21] showed a capacity around 1400 mAh/g at a current rate of 0.5 C for 700 cycles, with Coulombic efficiency >99.5% after 20 cycles. By comparison, we have reported the largest number of cycles (2000 cycles) with a capacity above 1000 mAh/g. In addition, our preparation of porous silicon nanostructure does not require high-temperature annealing[20] or chemical vapor deposition[21] and therefore may offer a potential cost benefit.

We note that a recent paper[30] reported that silicon nanoparticles (~100 nm) can achieve good cyclability (100 cycles) by using a special and possibly expensive alginate binder (viscosity >2000 cP at 1 wt %) synthesized in their own lab, and the authors attributed the improved cyclability to the high viscosity of their alginate binder. In contrast, here we used a commercially available alginate binder (Sigma Aldrich, cat. no. A2033) with lower viscosity (2000 cP at 2 wt %). We believe the significantly improved cyclability shown in Figure 3d,e mainly stems from the use of a porous silicon structure, while the use of commercial alginate also helped to a certain degree as compared to commonly used polyvinylidene fluoride (PVDF). Control experiments using commercial alginate binder on

dx.doi.org/10.1021/nl300206e | Nano Lett. 2012, 12, 2318−2323

silicon nanoparticles (Sigma Aldrich, around 100 nm) and using PVDF on porous silicon nanowires can be found in the Supporting Information.

To determine the morphology change of porous Si nanowires, several batteries after 10 cycles running at 0.1 C (0.4 A/g) were disassembled, and silicon anodes were washed with acetonitrile and 0.5 M HNO_3 to remove the SEI layer and then dissolved in ethanol to make samples for TEM observation. For clear comparison, Figure 4 shows the TEM image of a porous Si nanowire before (Figure 4a) and after cycling (Figure 4b,c). Figure 4b clearly shows that the nanowire remains highly porous, and the pore size does not change significantly after cycling (compared to Figure 4a). This agrees well with theoretical analysis showing that porous silicon with a large initial pore size and high porosity would not change its structure significantly after lithiation. Here the initial pore diameter was around 8 nm, and the wall between adjacent pores had a thickness of about 6 nm (Figure 4a); after cycling, the pore diameter and the wall thickness are still around 7−8 nm. The porous silicon nanowires are mostly amorphous (Figure 4c), with some dark dots less than 5 nm embedded in the amorphous matrix. SAED in Figure 4d confirms that the dots are crystalline silicon. Similar observation of small portion of unlithiated silicon was reported before,[17,20] and the underlying mechanism is not fully understood and deserves further investigation. This provides evidence that lithiation and delithiation in silicon is not homogeneous, therefore contributing to nonuniform stress distribution even at low charging/discharging rates. In some locations, accumulated stress may be large enough to break silicon into fragments. This is especially true for nonporous structures, like silicon nanowires, which are not able to sustain its capacity after long cycling, since lithium ions can only intercalate into silicon from the very outer surface and generate a large concentration gradient from surface to inner core, thus inducing large stress. In addition, low diffusivity of lithium ions in silicon generates a lithium ion concentration gradient that also compromises the capacity, as discussed with the simulation in Figure 1: the larger the concentration gradient, the lower the charge/discharge capacity. For porous silicon nanowires, the electrolyte goes everywhere in the pores, and lithium intercalation happens instantaneously wherever there is a contact between silicon and electrolyte. Previous study shows that CVD grown silicon nanowire can also become porous after lithiation and delithiation;[31] however, there is still capacity degradation after some cycles for CVD silicon nanowires.[11] As our simulation in Figure 1d shows, the stress in porous silicon after lithiation strongly depends on the porosity, which is understandable. We suspect that when CVD grown silicon nanowires become porous after several cycles, the resulting porosity and location of pores (surface of nanowires vs bulk of nanowires) can be different from ours, which might lead to the observed difference in the cycling performance. Here, we also believe that boron doping increases electron conductivity in silicon, which might help to reach a high capacity at high current rates, and the alginate, due to its high viscosity, could further improve the structural stability during cycling. Further experiments are currently under way to produce and test porous silicon nanowires with different pore sizes and porosities.

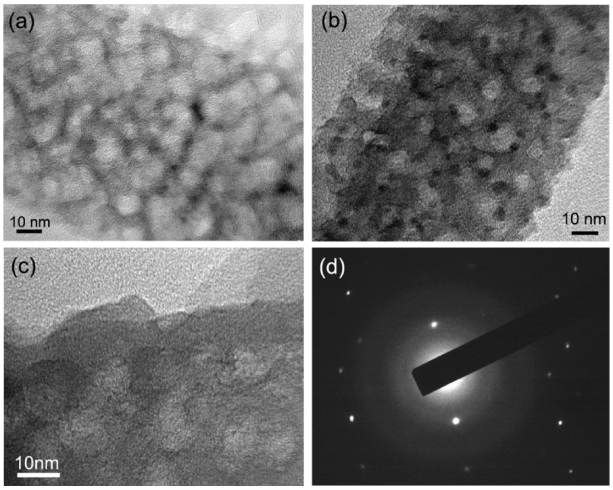

Figure 4. TEM images of silicon nanowires before (a) and after (b) lithiation after 10 cycles at a current rate of 0.4 A/g. (c) Enlarged TEM image of (b) showing the amorphous silicon structure. (d) SAED pattern showing black spots in (b) are crystalline silicon.

In conclusion, we have carried out both theoretical and experimental studies on using porous doped silicon nanowires for lithium ion battery applications. Our simulation shows porous silicon having a large pore size and high porosity can maintain its structure after lithium ion intercalation while having low stress, which is beneficial for getting high capacity and long cycle retention. Porous silicon nanowires were produced by direct etching of boron-doped silicon wafers and exhibited superior electrochemical performance and long cycle life as the anode material in lithium ion battery with alginate used as binder. The capacity remained stable above 2000, 1600, and 1100 mAh/g at current rates of 2, 4, and 18 A/g, respectively, even after 250 cycles. We believe the good cyclability mainly stems from the use of a porous silicon structure, while the use of a commercial alginate binder also helped to a certain degree as compared to commonly used polyvinylidene fluoride (PVDF). Our work demonstrates the great potential of porous silicon structures for energy storage applications.

■ ASSOCIATED CONTENT

Supporting Information

Additional information for methods used in simulation and fabrication of porous silicon nanowire anode. Control experimental results of using alginate binder on silicon nanoparticles and PVDF binder on porous silicon nanowires. This material is available free of charge via the Internet at http://pubs.acs.org.

■ AUTHOR INFORMATION

Corresponding Author

*chongwuz@usc.edu

Author Contributions

[§]These authors contributed equally.

Notes

The authors declare no competing financial interest.

■ ACKNOWLEDGMENTS

We acknowledge the University of Southern California for financial support.

REFERENCES

(1) Li, H.; Wang, Z. X.; Chen, L. Q.; Huang, X. J. *Adv. Mater.* **2009**, *21* (45), 4593−4607.
(2) Arico, A. S.; Bruce, P.; Scrosati, B.; Tarascon, J. M.; Van Schalkwijk, W. *Nat. Mater.* **2005**, *4* (5), 366−377.
(3) Choi, N. S.; Yao, Y.; Cui, Y.; Cho, J. *J. Mater. Chem.* **2011**, *21* (27), 9825−9840.
(4) Kasavajjula, U.; Wang, C. S.; Appleby, A. J. *J. Power Sources* **2007**, *163* (2), 1003−1039.
(5) Tarascon, J. M.; Armand, M. *Nature* **2001**, *414* (6861), 359−367.
(6) Scrosati, B. *Nature* **1995**, *373* (6515), 557−558.
(7) Nikolaev, V. P.; Morachevskii, A. G.; Demidov, A. I.; Bairachnyi, E. V. *Russ. J. Appl. Chem.* **1980**, *53* (9), 1549−1551.
(8) Boukamp, B. A.; Lesh, G. C.; Huggins, R. A. *J. Electrochem. Soc.* **1981**, *128* (4), 725−729.
(9) Takamura, T.; Ohara, S.; Uehara, M.; Suzuki, J.; Sekine, K. *J. Power Sources* **2004**, *129* (1), 96−100.
(10) Yin, J. T.; Wada, M.; Yamamoto, K.; Kitano, Y.; Tanase, S.; Sakai, T. *J. Electrochem. Soc.* **2006**, *153* (3), A472−A477.
(11) Chan, C. K.; Peng, H. L.; Liu, G.; McIlwrath, K.; Zhang, X. F.; Huggins, R. A.; Cui, Y. *Nat. Nanotechnol.* **2008**, *3* (1), 31−35.
(12) Peng, K. Q.; Jie, J. S.; Zhang, W. J.; Lee, S. T. *Appl. Phys. Lett.* **2008**, *93* (3), 033105−033107.
(13) Cui, L.-F.; Yang, Y.; Hsu, C.-M.; Cui, Y. *Nano Lett.* **2009**, *9* (9), 3370−3374.
(14) Liu, X. H.; Zhang, L. Q.; Zhong, L.; Liu, Y.; Zheng, H.; Wang, J. W.; Cho, J.-H.; Dayeh, S. A.; Picraux, S. T.; Sullivan, J. P.; Mao, S. X.; Ye, Z. Z.; Huang, J. Y. *Nano Lett.* **2011**, *11* (6), 2251−2258.
(15) Dimov, N.; Kugino, S.; Yoshio, M. *Electrochim. Acta* **2003**, *48* (11), 1579−1587.
(16) Kim, H.; Seo, M.; Park, M.-H.; Cho, J. *Angew. Chem., Int. Ed.* **2010**, *49* (12), 2146−2149.
(17) Park, M. H.; Kim, M. G.; Joo, J.; Kim, K.; Kim, J.; Ahn, S.; Cui, Y.; Cho, J. *Nano Lett.* **2009**, *9* (11), 3844−3847.
(18) Song, T.; Xia, J.; Lee, J.-H.; Lee, D. H.; Kwon, M.-S.; Choi, J.-M.; Wu, J.; Doo, S. K.; Chang, H.; Il Park, W.; Zang, D. S.; Kim, H.; Huang, Y.; Hwang, K.-C.; Rogers, J. A.; Paik, U. *Nano Lett.* **2010**, *10* (5), 1710−1716.
(19) Zhou, S.; Wang, D. W. *ACS Nano* **2010**, *4* (11), 7014−7020.
(20) Kim, H.; Han, B.; Choo, J.; Cho, J. *Angew. Chem., Int. Ed.* **2008**, *47* (52), 10151−10154.
(21) Yao, Y.; McDowell, M. T.; Ryu, I.; Wu, H.; Liu, N.; Hu, L.; Nix, W. D.; Cui, Y. *Nano Lett.* **2011**, *11* (7), 2949−2954.
(22) Wang, X. L.; Han, W. Q. *ACS Appl. Mater. Inter.* **2010**, *2* (12), 3709−3713.
(23) Sun, C. Y.; Qin, C.; Wang, C. G.; Su, Z. M.; Wang, S.; Wang, X. L.; Yang, G. S.; Shao, K. Z.; Lan, Y. Q.; Wang, E. B. *Adv. Mater.* **2011**, *23*, (47), 5629.
(24) Obrovac, M. N.; Christensen, L. *Electrochem. Solid-State Lett.* **2004**, *7* (5), A93−A96.
(25) Zhang, X.; Shyy, W.; Sastry, A. M. *J. Electrochem. Soc.* **2007**, *154* (10), A910−A916.
(26) Park, J.; Lu, W.; Sastry, A. M. *J. Electrochem. Soc.* **2011**, *158* (2), A201−A206.
(27) Qu, Y.; Zhou, H.; Duan, X. *Nanoscale* **2011**, *3* (10), 4060−4068.
(28) Hochbaum, A. I.; Gargas, D.; Hwang, Y. J.; Yang, P. *Nano Lett.* **2009**, *9* (10), 3550−3554.
(29) Li, J.; Dahn, J. R. *J. Electrochem. Soc.* **2007**, *154* (3), A156−A161.
(30) Kovalenko, I.; Zdyrko, B.; Magasinski, A.; Hertzberg, B.; Milicev, Z.; Burtovyy, R.; Luzinov, I.; Yushin, G. *Science* **2011**, *333* (6052), 75−79.
(31) Choi, J. W.; McDonough, J.; Jeong, S.; Yoo, J. S.; Chan, C. K.; Cui, Y. *Nano Lett.* **2010**, *10*, 1409−1413.